Probing metal-molecule contact at the atomic scale via conductance jumps

Biswajit Pabi ⬤, Debayan Mondal ⬤, Priya Mahadevan,* and Atindra Nath Pal ⬤†

Department of Condensed Matter Physics and Material Sciences, S. N. Bose National Centre for Basic Sciences,
Sector III, Block JD, Salt Lake, Kolkata 700106, India

Understanding the formation of metal-molecule contact at the microscopic level is the key towards controlling and manipulating atomic-scale devices. Employing two isomers of bipyridine, $4, 4'$ bipyridine and $2, 2'$ bipyridine between gold electrodes, here, we investigate the formation of a metal-molecule bond by studying charge transport through single molecular junctions using a mechanically controlled break junction technique at room temperature. While both molecules form molecular junctions during the breaking process, closing traces show the formation of molecular junctions unambiguously for $4, 4'$ bipyridine via a conductance jump from the tunneling regime, referred to as "jump to molecular contact," being absent for $2, 2'$ bipyridine. Through statistical analysis of the data, along with molecular dynamics and first-principles calculations, we establish that contact formation is strongly connected with the molecular structure of the electrodes as well as how the junction is broken during the breaking process, providing important insights for using a single molecule in an electronic device.

DOI: [10.1103/PhysRevB.104.L121407](https://doi.org/10.1103/PhysRevB.104.L121407)

I. INTRODUCTION

The drive towards miniaturization has led to envisaged electronic components having elements which have dimensions in the nanometer scale. These elements could be molecules [1], and before placing them in a circuit, it becomes essential to know how they would behave. While there have been tremendous advances made [2–5], probing the contact formation at the microscopic level has not been straightforward. A route towards exploring atomic-scale transport has involved forming mechanical break junctions [6]. Considering metallic electrodes, examining the metal-metal contact formed in a break junction at liquid helium temperatures, one finds a regime in which one has quantum tunneling, followed by the formation of contacts. This transition from a tunneling transport regime to contact formation occurs, in most cases, via a sudden jump in the conductance, referred to as a jump to contact [7,8]. Various metals like Au, Pt, Cu, and Ag exhibit a jump to contact, while there are others like Ir, Ni, and W in which a jump to contact can be absent. In a controlled experiment involving an Au break junction, using a highly ordered gold electrode, it was shown that the phenomena could be explained by a generic potential energy model with the elastic constant of the metal being the only free parameter [9].

The formation of a metal-molecule bond is rather complex and highly dependent on the nature of binding groups and the geometry of the electrodes [10–17]. A jump to molecular contact was reported for several flat molecules through scanning tunneling microscopy based experiments at cryogenic temperatures [18–21]. It is believed that there exist two energetically close adsorption geometries with one of them bridging the junction via a soft phonon from the molecular side groups [19]. In the case of mechanically controllable break junctions, however, the shapes of the electrodes are not expected to remain in line while approaching each other, especially at room temperature [22]. This may lead to the formation of asymmetric junctions, which, in contrast to the breaking process, may not provide precise conductance of single molecular junctions. In recent break junction experiments with an organometallic compound, carried out in solution, a jump was observed in the conductance for closing traces [23]. This was attributed to the formation of one-dimensional coordination polymers in those junctions. The knowledge about the role of metal-molecule interaction towards bond formation is rather limited and a general picture is still lacking.

In the present study, we report the observation of jump to molecular contact in a single molecular junction by studying the charge transport using a mechanically controllable break junction setup at ambient temperature. Through statistical analysis of conductance-distance traces, along with density functional theory based calculations and *ab initio* molecular dynamics, we provide the microscopic origin behind the metal-molecular contact formation. Considering two isomers of bipyridine, $4, 4'$ bipyridene ($4, 4'$-BPY) and $2, 2'$ bipyridene ($2, 2'$-BPY), attached to gold electrodes, we find that molecular junctions form in the breaking traces for both the molecules. The surprising aspect is that $4, 4'$-BPY forms molecular junctions isotropically with conductance jumps in the closing traces also, an aspect that is absent for $2, 2'$-BPY. Our density functional theory (DFT) and molecular dynamics (MD) simulations reveal two important mechanisms for jump to molecular contact. Firstly, while the $2, 2'$-BPY prefers to lie flat on the Au surface, $4, 4'$-BPY has two stable minima—one with the molecule lying flat on the surface and the other with

the molecule standing vertically, despite having a similar anchoring group involving nitrogen. This unusual aspect of the 4, 4′-BPY emerges from the fact that the nitrogen forms a very strong bond in 4, 4′-BPY [24] while the orientation on the Au surface in 2, 2′-BPY does not allow a similar strong bond due to steric effects from the hydrogens attached to the carbon atoms, with the Au-N bond length equal to 2.24 Å here in contrast to 2.12 Å for the 4, 4′-BPY molecule. The possibility of having two stable energy conformations may lead to a jump to contact for 4, 4′-BPY, similar to Ref. [19]. Additionally, we propose another mechanism, according to which, the observed jump to molecular contact in the case of 4, 4′-BPY may arise from the fact that the molecule breaks by pulling a few gold atoms with it due to a strong Au-N bond compared to the Au-Au bond. Consequently, while making the contacts during the closing loops, one does not have to worry about the directionality of the bonding. Through a statistical analysis of the experimental data the second mechanism was found to be the dominant one.

II. METHODS

A single molecular junction was formed in a custom-built mechanically controllable break junction (MCBJ) technique at ambient condition [25]. A gold wire (0.1 mm diameter, 99.998%; Alfa Aesar) with a notch at its center was fixed onto a flexible substrate (phosphor bronze) with a two-component epoxy glue (Stycast 2850 FT with catalyst 9). For creating molecular junctions, molecules (4, 4′-BPY and 2, 2′-BPY, 98%; Alfa Aesar) were either evaporated or drop casted (0.1 mM ethanol solution) on top of the notch and the wire was controllably broken using a piezo stack. The formation of molecular junctions was confirmed from the appearance of additional peaks in the conductance histograms below $1G_0$ (where $G_0 = 2e^2/h$ is the quantum of conductance). In the conductance-distance measurements, the typical moving rate of the piezo was 3.2 μm/s, which translates into an opening and respective closing rate for the two leads of about 2–4 nm/s (attenuation factor of $\sim 10^{-3}$) [26].

In order to model the experiments, we use density functional theory based *ab initio* electronic structure calculations using the generalized gradient approximation (Perdew-Burke-Ernzerhof) [27] for the exchange-correlation functional with dispersion corrections (DFT-D2) [28,29] as implemented within the Vienna *ab initio* simulation package (VASP) [30–33]. We have used Γ point k-space sampling [34] and a plane-wave cutoff of 500 eV. The structural relaxations were carried out until forces were less than 10^{-3} eV/atom and energy convergence in each case was 10^{-5} eV. The *ab initio* MD simulations [33,35,36] were carried out at room temperature (300 K) and the whole system is kept at the desired temperature in an *NVT* canonical ensemble using a Nosé-Hoover thermostat [37–39] for several molecular junctions formed by 4, 4′-BPY and 2, 2′-BPY molecules with gold electrodes. The optimized structure of a gold slab–molecule–gold slab is used to construct the junction atomic geometry, where eight layers were used to construct the slab. The slabs are separated by a vacuum of 15 Å. The electrodes are pulled apart in steps of 0.1 Å. The entire system is relaxed at every step by taking 200 MD steps of 0.5 fs.

III. RESULTS AND DISCUSSION

Typical opening or pull (blue) and closing or push (red) conductance traces for both the molecules are shown in Figs. 1(b) and 1(d), respectively (see Supplemental Material [40] for measurement details; also see [41]). During the junction breaking process (pull), well-developed molecular plateaus in the range of 10^{-3}–$10^{-4}G_0$ is noticed for both 4, 4′-BPY and 2, 2′-BPY. Closing traces (push) of 4, 4′-BPY, however, exhibit a plateaulike feature which is longer and slanted compared to the pull traces, in line with the previous observations [42]. In the case of 2, 2′-BPY, no such plateau was observed in push traces; instead, a continuous tunneling-like behavior was observed. A closer look at the push traces for 4, 4′-BPY reveals that atomic contacts of Au form via two jumps in the conductance: the first jump occurring from the background noise or tunneling to a conductance value of $\sim 10^{-3}G_0$ and the second one from $\sim 0.1G_0$ to a few tenths of G_0. The first jump is referred to as "jump to molecular contact" (abbreviated as J2C) and the second jump corresponds to the formation of metallic contact. No such jump is observed in the case of 2, 2′-BPY. In the following paragraphs we discuss more details about the origin of the J2C phenomena.

Thousands of individual traces were collected, analyzed, and plotted as histograms to get a meaningful estimate of the molecular conductance from statistically independent junction configurations. Figures 1(c) and 1(e) display the logarithmically binned normalized one-dimensional (1D) conductance histogram for 4, 4′-BPY and 2, 2′-BPY, respectively, constructed from 5000 and 8000 conductance traces without any data selection. For both the molecules, the pull histogram (blue) exhibits a clear peak around $1G_0$ corresponding to the Au atomic contact, followed by a prominent molecular conductance feature in the range of $5\times10^{-2}G_0$ to $5\times10^{-4}G_0$ (4, 4′-BPY) and $1\times10^{-3}G_0$ to $1\times10^{-4}G_0$ (2, 2′-BPY). For 4, 4′-BPY, the conductance peak can be resolved into two separate peaks ($9.33 \pm 0.29\times10^{-4}G_0$ and $4.28 \pm 0.07\times10^{-4}G_0$), obtained by fitting Gaussian to the characteristic maxima, similar to the previous observation [43,44] (see Fig. S5 in the Supplemental Material [40] for details; also see [43,45]). The most probable conductance for 2, 2′-BPY was found to be $1.27 \pm 0.05\times10^{-4}G_0$ [Fig. 1(e)]. The push histogram (red) for 4, 4′-BPY [Fig. 1(c)] shows a clear conductance peak in the region ($5\times10^{-4}G_0$ to $2\times10^{-1}G_0$), being higher than the pull conductance, whereas, no such conductance peak is observed in the case of 2, 2′-BPY.

To get a clear picture about the evolution of conductance during the formation processes and understand the possible origin of the observed J2C in the case of 4, 4′-BPY, we have constructed a conductance-displacement histogram from the push traces for both the molecules. Figures 2(a) and 2(b) display such 2D histograms for the push data for 4, 4′-BPY and 2, 2′-BPY, respectively. The plots were constructed from the same traces used in the 1D histogram, by aligning them at $2G_0$ and having 100 bins per decade. Corresponding pull histograms are shown in the Supplemental Material [40] (see Fig. S2). By analyzing the length histogram, we see that 4, 4′-BPY [Fig. 2(a)] exhibits a longer and slanted conductance plateau in push with an average length of 9.77 ± 0.05 Å [see Fig. S3(c) in the Supplemental Material [40]], compared
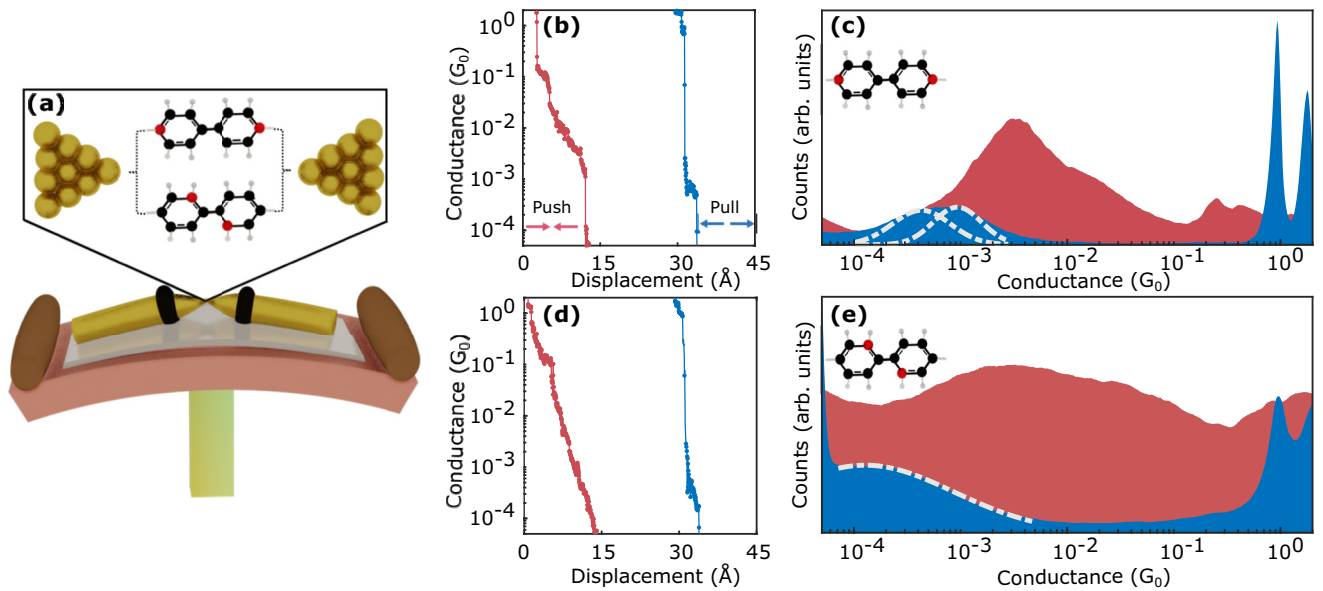
FIG. 1. (a) Schematic of a mechanically controllable break junction (MCBJ) set up, along with the schematic representation of the molecules used in this work: $4, 4'$ bipyridine ($4, 4'$-BPY) and $2, 2'$ bipyridine ($2, 2'$-BPY). Conductance traces for (b) $4, 4'$-BPY and (d) $2, 2'$-BPY. Blue (red) represents trace during pull (push). 1D logarithmic conductance histogram for (c) $4, 4'$-BPY and (e) $2, 2'$-BPY, constructed from 5000 and 8000 traces, respectively, without any data selection. Blue and red represent the corresponding pull and push, respectively. White dashed line shows the Gaussian fit to the corresponding molecular peaks of the histogram.

to the corresponding pull plateaus with an average plateau length of 3.03 ± 0.02 Å [see Fig. S3(a) in the Supplemental Material [40]]. A similar analysis for $2, 2'$-BPY (pull) shows an average plateau length of 2.57 ± 0.01 Å [see Fig. S3(b) in the Supplemental Material [40]]. The most intriguing aspect is the unambiguous formation of a single molecular junction for $4, 4'$-BPY during the closing process with a conductance jump occurring mostly at $\sim (5.98 \pm 0.23) \times 10^{-4} G_0$, calculated from the Gaussian fit of the histogram of conductance

values where jump to molecular contact takes place, shown in the inset of Fig. 2(a) (see Supplemental Material [40] for details about the jump detection algorithm). This value bears a close resemblance to the conductance of Au-$4, 4'$-BPY-Au junctions in the stretched configuration, reported earlier [43]. Jump to molecular contact is clearly absent for $2, 2'$-BPY [Fig. 2(b)], where a continuous tunneling slope is observed from the noise background while closing the electrodes and no clear formation of molecular junction was noticed.
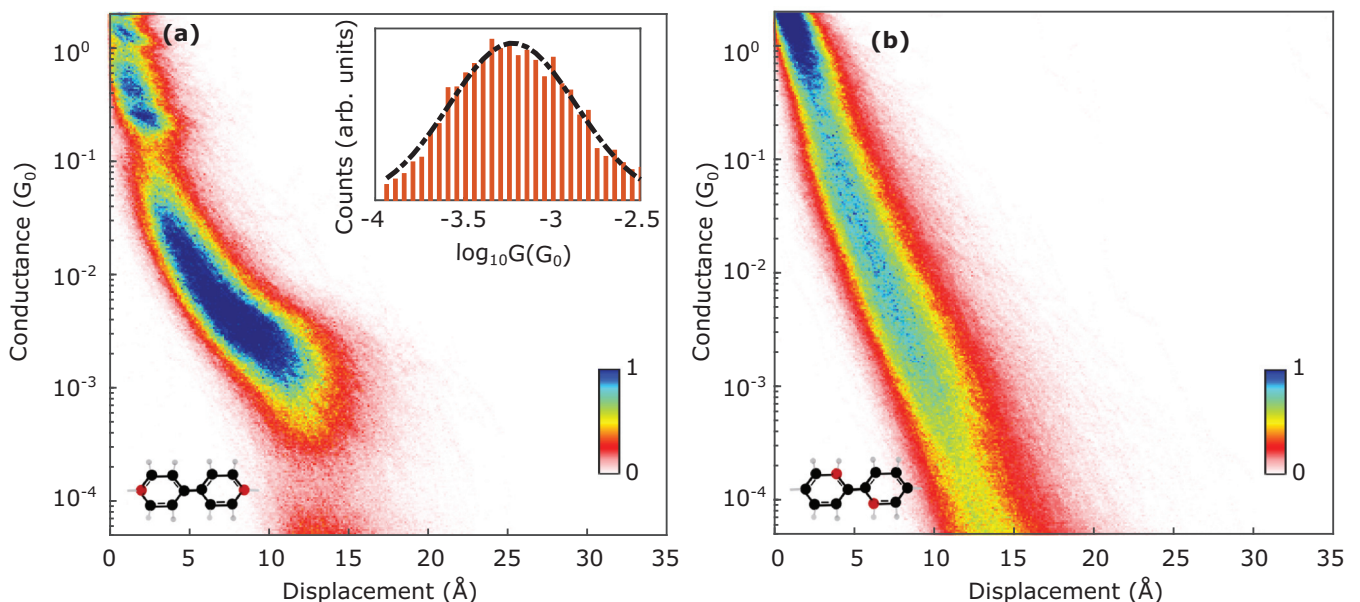

FIG. 2. 2D Conductance-displacement density plot for (a) $4, 4'$-BPY and (b) $2, 2'$-BPY, for push traces used in Figs. 1(c) and 1(e), with 100 bins per decade. Inset: Histogram of the conductance of the molecular contact formed after the jump, having 3750 traces (see Supplemental Material [40] for details).
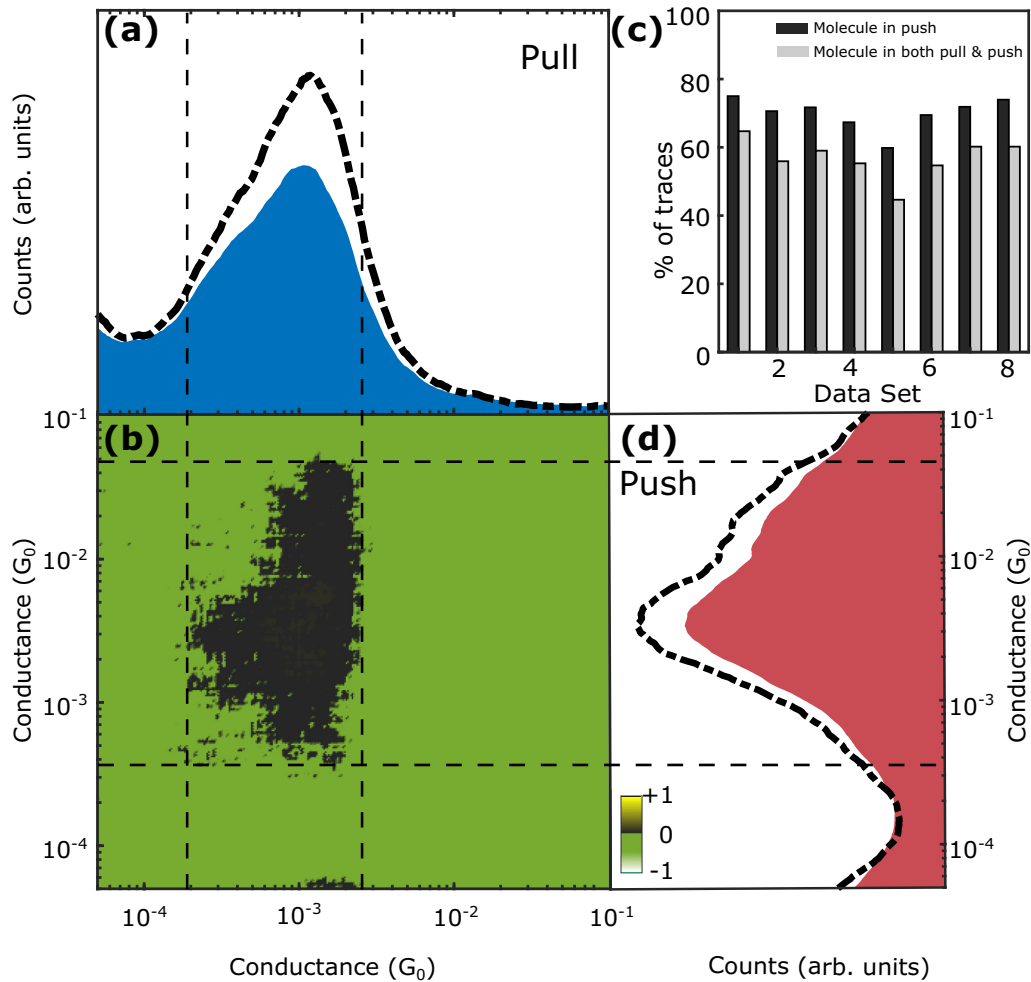
FIG. 3. Conditional histogram of 4, 4′-BPY for (a) pull and (d) push traces. The black dash-dotted line represents the histogram of the selected pull (push) traces for which plateaus are formed in the corresponding push (pull) traces, respectively. The blue and red area graph represents the histogram for all traces, as a reference for (a) and (d), respectively. (b) 2D correlation histogram, indicating the correlation between the pull (horizontal axis) and push (vertical axis). The histogram is constructed from 10 000 traces without any data selection using 50 bins per decade. (c) Bar diagram showing the percentage of traces forming a molecular junction in push via jump (black) and the percentage of traces having both molecules in the pull and push (gray) for eight different data sets.

A statistical correlation analysis of the conductance traces, as described in Ref. [45], has been used to distinguish various structural configurations and understand their origin. Using the same procedure, we have carried out a statistical correlation analysis between the pull and push traces [46] to find out if there is any possible correlation between them (see Supplemental Material [40] for details; also see [12,45–49]). Figure 3(b) shows the two-dimensional cross correlation plot for 4, 4′-BPY, constructed from 10 000 traces with 50 logarithmic bins per decade. The vertical axis belongs to the push traces and the horizontal to the corresponding pull traces. A clear positive correlation between the pull and corresponding push traces is observed, shown by a dark spot near the region where the pull and push peaks appear, as depicted by the black dashed lines. This is also evident from the conditional histogram of the corresponding pull (push) traces, shown by the black dash-dotted line in Figs. 3(a) [3(d)]. While selecting the push (pull) traces having a conductance plateau in the selected region between the black dashed lines, we observe a clear enhancement in the conductance peak of the pull (push)

histogram. A positive correlation may indicate a structural memory effect [49] that any molecular junction in push is possible, mostly when a molecular junction is formed during the breaking process (pull). A similar positive correlation between pull and push traces was observed for the Au-CO-Au junction at cryogenic temperature [50]. It was concluded that the molecule is bound rigidly to the apex of one electrode and a similar single molecular configuration was reestablished during the closing process. At room temperature, however, due to the enhanced surface diffusion, electrodes are flattened and a correlation between the opening and closing traces is uncommon. Figure 3(c) compares the correlation observed in push from eight different data sets from three different samples with a varying probability of molecular junction formation. A conditional analysis of eight statistically independent data sets indicates that J2C was observed for more than 80% of the cases whenever a molecular junction is formed during pull, establishing the fact that J2C is primarily associated with the formation of a molecular junction in pull (see Supplemental Material [40] for details).
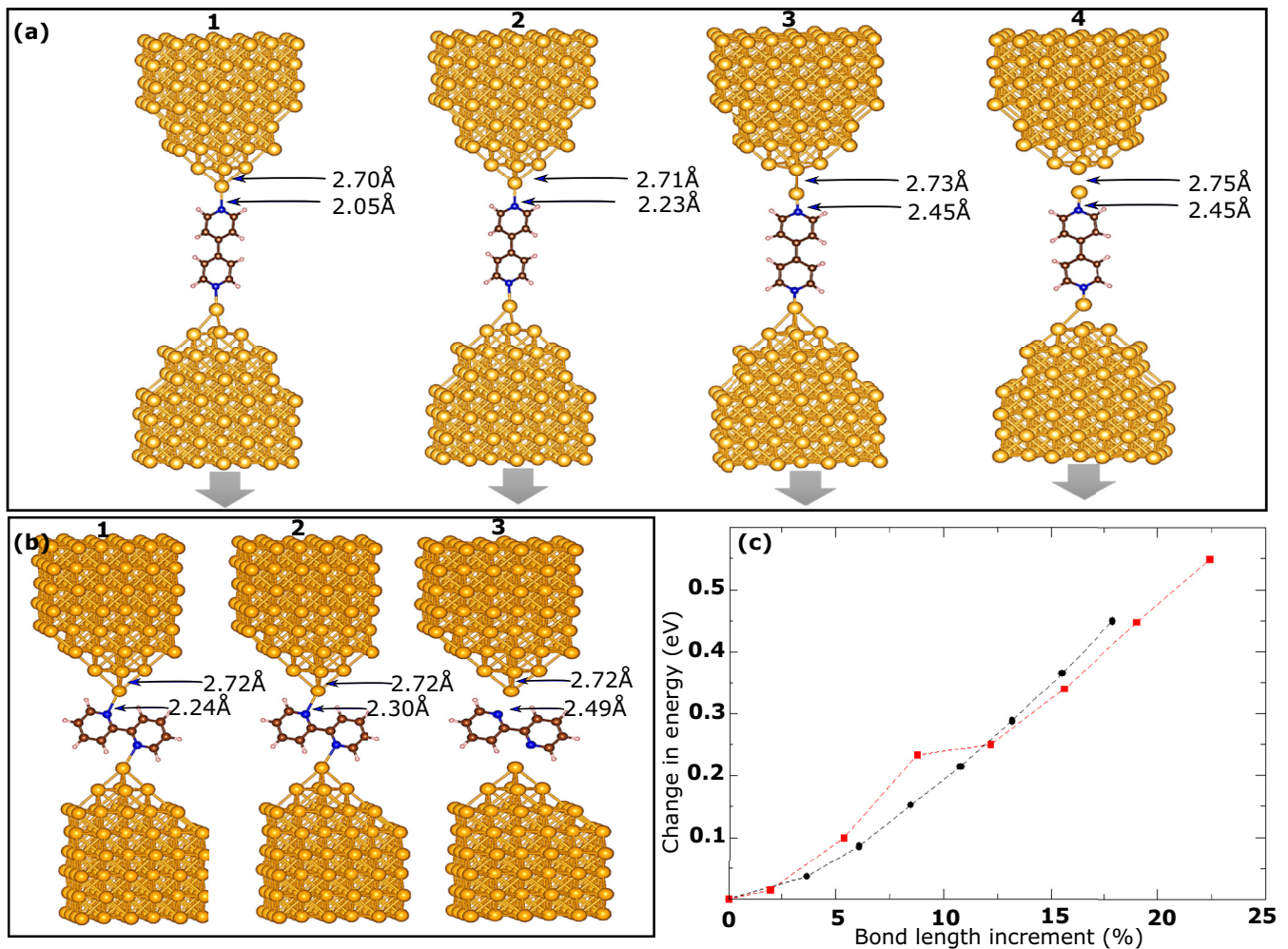
FIG. 4. (a) MD snapshot of molecular junction with 4, 4′-BPY for effective length of electrode (1) 11.10 Å, (2) 11.60 Å, (3) 12.20 Å, and (4) 12.45 Å. (b) MD snapshot of molecular junction with 2, 2′-BPY for effective length of electrode (1) 6.65 Å, (2) 6.80 Å, and (3) 6.89 Å. (c) Change in total energy with respect to stretching of the bond of molecule-Au (black) and Au-Au atom (red).

To simulate the experiment, we take two pyramidal gold electrodes and place the molecule 4, 4′-BPY symmetrically between the electrodes. The optimized Au-molecule bond length was found to be 2.12 Å in the static calculation. Placing the molecule at this distance from the electrode led to an effective length (distance between two electrode tips) of 11.10 Å. The Au-Au bond lengths in the electrodes were set equal to the bond length of 2.65 Å found in the experimental structure. Molecular dynamics simulations were then carried out at a temperature of 300 K. After 200 iterations, we find that while the positions of the Au atoms in the electrode do not change, two atoms from the electrode come closer to the molecule making shorter bonds. We have increased the effective length to several values as shown in Fig. 4(a) and there are two aspects that emerge. An Au atom gets removed from the electrode and moves towards the molecule. Additionally the molecule is no longer symmetrically placed with respect to electrodes, and the distance of the molecule and one end of the electrode becomes shorter (on one side the length is 2.45 Å and on the other it is 2.55 Å). The converged effective length is now 12.20 Å [Fig. 4(a), 3]. If we increase the effective length further (13.00 Å), we still find that the Au atom moves towards

the molecule [Fig. 4(a), 4]. A similar calculation was done for 2, 2′-BPY. The N-Au bond length is found to be 2.24 Å where we optimized the structure at 0 K. When we increase the separation, the Au atom from the electrode is not detached as found for 4, 4′-BPY [Fig. 4(b)].

In order to understand this further, we have examined the energy variations as we stretch the Au-Au bond of a metal-metal contact. The energy is found to vary continuously until a bond length of 3.20 Å (a stretch of 8.8% in the bond length) [Fig. 4(c)]. At this point there is a discontinuous change in the bond length and a jump in the energy also. The energy variations now lie on a new curve and are again continuous. As the hopping interaction strength between any two atoms varies inversely with their distance according to a power law, this jump in bond length would translate into a jump in the hopping interaction strength. This then leads to a jump in the conductance, and is consistent with experiments carried out with Au electrodes in which a jump to contact is observed [7–9]. When we went on to examine the variations in the energy of the molecule connected to a Au atom, on subjecting it to a similar elongation we found a continuous variation [Fig. 4(c)]. This suggests that one should see only a monotonic
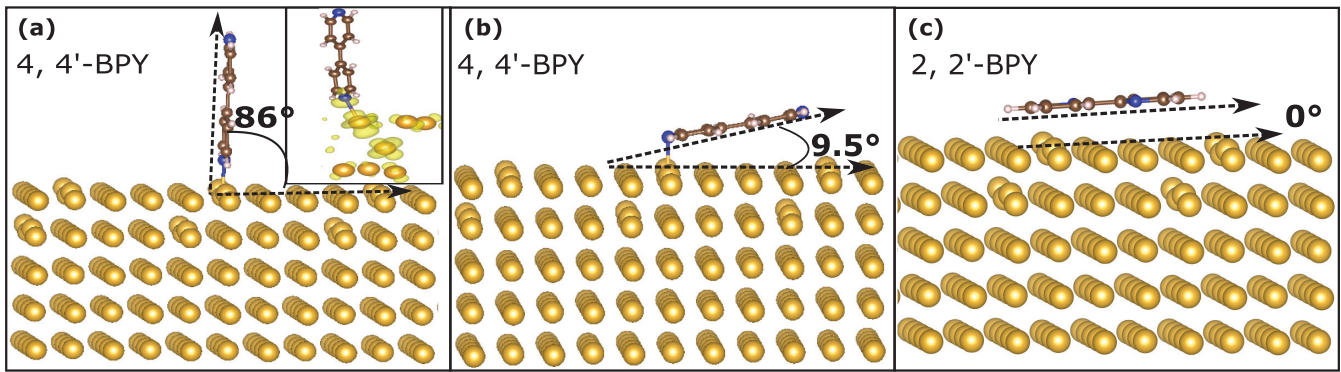
FIG. 5. Complete optimized structure for vertically aligned and horizontally aligned orientations of the molecules shown in panels (a) and (b) for 4, 4′-BPY and in panel (c) for 2, 2′-BPY. Charge density of a state formed as a result of interactions between Au and the molecule (see Fig. S7 in the Supplemental Material [40]) is shown in the inset of panel (a).

variation in the conductivity in this case. This is, however, contrary to experiments where one has a jump to contact.

To shed more light on this, we have placed both molecules on gold surface and carried out static calculations for different orientations of both molecules at a fixed distance. These results suggest that there are two minima present for 4, 4′-BPY on gold, while there is only one minima for the 2, 2′-BPY. Allowing for a complete structural optimization in each case leads to the orientations of the molecules shown in panels (a) and (b) of Fig. 5 for 4, 4′-BPY and what is shown in panel (c) for 2, 2′-BPY. While in panel (a) we find that the molecule prefers an orientation almost vertical to the surface, in (b) and (c) we find that the molecule likes to lie horizontal to the surface. The reason for this is easy to understand. In the horizontal position the molecule interacts through the carbon backbone with the Au surface. Hence for both molecules, this corresponds to a stable orientation. In the vertical orientation, 4, 4′-BPY interacts strongly through the nitrogen with Au surface. This is evident from the charge density shown in the inset of Fig. 5(a), where one finds significant weight on several Au atoms beyond its nearest neighbor. In contrast the Au-N bond length is much longer for 2, 2′-BPY and found to be 2.24 Å as the steric effects from the neighboring atoms do not allow the molecule to come closer to the Au surface. This leads to only one stable minima for 2, 2′-BPY. The strong bonding interaction of the nitrogen in 4, 4′-BPY that we find is extremely directional. This would therefore imply that in the push cycle, we would not have the desired reproducibility as only certain orientations would form strong bonds. However, as we saw in the MD simulations and also supported by an analysis of the charge density of the bonding state between 4, 4′-BPY and the Au surface, we find the interaction between them to be strong enough to pull one or more Au atoms out. This then leads to a contact between two Au atoms in the push cycle; needless to say, the bonding between Au atoms involves *s* orbitals and is isotropic (it does not need to attach back to its initial position, and can attach with any other gold atom) [7,51,52], and hence we have the reproducibility. From Fig. 3(c) we observe that a jump to contact is observed in ∼20% cases despite not forming any molecular junction during pull. As we found that 4, 4′-BPY has two stable orientations on the Au surface, a jump may occur between them via a soft phonon mode of the molecule during push [19].

IV. CONCLUSION

In conclusion, we have studied the formation and the post rupture evolution of molecular junctions at room temperature of two isomers of bipyridene (4, 4′-BPY and 2, 2′-BPY) having the same anchoring groups using MCBJ techniques. Transport measurements indicate the formation of a stable molecular junction during the opening cycle for both of these molecules. During the closing cycle, however, we see that 4, 4′-BPY shows a clear formation of a molecular junction via a jump in the conductance from the tunneling regime, while a continuous quantum tunnelinglike behavior was observed for 2, 2′-BPY. As such formations of molecular junctions via a jump in the conductance at room temperature are rare, we use DFT calculations as well as *ab initio* MD simulations to explain them. Two possible mechanisms have come out from our study. Firstly, 4, 4′-BPY was found to have two possible conformations on the Au surface due to the formation of a strong Au-N bond, whereas, 2, 2′-BPY prefers to lay flat on the Au surface. These two stable conformations of 4, 4′-BPY may provide jump to contact while approaching the two electrodes. Secondly, we show that while breaking the Au-4, 4′-BPY junctions, primarily it is the Au-Au bond that is ruptured instead of the molecule-Au bond. As the Au atom attached to the molecule can bind isotropically with the other Au atoms of the electrodes, one has single molecular junctions formed during the closing process via conductance jumps similar to what one has seen for Au-Au contacts. Statistical analysis of our experimental data indicates that the second mechanism is the more dominant one in our case. We provide an important insight, describing the role of metal-molecule interaction on the formation of chemical bonds, important for the development of molecular-scale electronics.

[1] A. Aviram and M. A. Ratner, Molecular rectifiers, Chem. Phys. Lett. **29**, 277 (1974).

[2] B. Capozzi, J. Xia, O. Adak, E. J. Dell, Z.-F. Liu, J. C. Taylor, J. B. Neaton, L. M. Campos, and L. Venkataraman, Single-molecule diodes with high rectification ratios through environmental control, Nat. Nanotechnol. **10**, 522 (2015).

[3] R. Hayakawa, M. A. Karimi, J. Wolf, T. Huhn, M. S. Zoellner, C. Herrmann, and E. Scheer, Large magnetoresistance in single-radical molecular junctions, Nano Lett. **16**, 4960 (2016).

[4] L. Cui, S. Hur, Z. A. Akbar, J. C. Klöckner, W. Jeong, F. Pauly, S.-Y. Jang, P. Reddy, and E. Meyhofer, Thermal conductance of single-molecule junctions, Nature (London) **572**, 628 (2019).

[5] A. N. Pal, D. Li, S. Sarkar, S. Chakrabarti, A. Vilan, L. Kronik, A. Smogunov, and O. Tal, Nonmagnetic single-molecule spin-filter based on quantum interference, Nat. Commun. **10**, 5565 (2019).

[6] J. M. Krans, C. J. Muller, I. K. Yanson, T. C. M. Govaert, R. Hesper, and J. M. van Ruitenbeek, One-atom point contacts, Phys. Rev. B **48**, 14721 (1993).

[7] C. Untiedt, M. J. Caturla, M. R. Calvo, J. J. Palacios, R. C. Segers, and J. M. van Ruitenbeek, Formation of a Metallic Contact: Jump to Contact Revisited, Phys. Rev. Lett. **98**, 206801 (2007).

[8] L. Gerhard and W. Wulfhekel, Conductance and adhesion in an atomically precise Au-Au point contact, Phys. Rev. B **101**, 035429 (2020).

[9] M. L. Trouwborst, E. H. Huisman, F. L. Bakker, S. J. van der Molen, and B. J. van Wees, Single Atom Adhesion in Optimized Gold Nanojunctions, Phys. Rev. Lett. **100**, 175502 (2008).

[10] Y. S. Park, A. C. Whalley, M. Kamenetska, M. L. Steigerwald, M. S. Hybertsen, C. Nuckolls, and L. Venkataraman, Contact chemistry and single-molecule conductance: A comparison of phosphines, methyl sulfides, and amines, J. Am. Chem. Soc. **129**, 15768 (2007).

[11] L. Venkataraman, J. E. Klare, I. W. Tam, C. Nuckolls, M. S. Hybertsen, and M. L. Steigerwald, Single-molecule circuits with well-defined molecular conductance, Nano Lett. **6**, 458 (2006).

[12] M. Kamenetska, M. Koentopp, A. C. Whalley, Y. S. Park, M. L. Steigerwald, C. Nuckolls, M. S. Hybertsen, and L. Venkataraman, Formation and Evolution of Single-Molecule Junctions, Phys. Rev. Lett. **102**, 126803 (2009).

[13] F. Chen, X. Li, J. Hihath, Z. Huang, and N. Tao, Effect of anchoring groups on single-molecule conductance: Comparative study of thiol-, amine-, and carboxylic-acid-terminated molecules, J. Am. Chem. Soc. **128**, 15874 (2006).

[14] G. Pera, S. Martín, L. M. Ballesteros, A. J. Hope, P. J. Low, R. J. Nichols, and P. Cea, Metal–molecule–metal junctions in Langmuir-Blodgett films using a new linker: Trimethylsilane, Chem. Eur. J. **16**, 13398 (2010).

[15] S. Kaneko, R. Takahashi, S. Fujii, T. Nishino, and M. Kiguchi, Controlling the formation process and atomic structures of single pyrazine molecular junction by tuning the strength of the metal–molecule interaction, Phys. Chem. Chem. Phys. **19**, 9843 (2017).

[16] R. Vardimon, T. Yelin, M. Klionsky, S. Sarkar, A. Biller, L. Kronik, and O. Tal, Probing the orbital origin of conductance oscillations in atomic chains, Nano Lett. **14**, 2988 (2014).

[17] A. N. Pal, T. Klein, A. Vilan, and O. Tal, Electronic conduction during the formation stages of a single-molecule junction, Beilst. J. Nanotechnol. **9**, 1471 (2018).

[18] W. Haiss, C. Wang, I. Grace, A. S. Batsanov, D. J. Schiffrin, S. J. Higgins, M. R. Bryce, C. J. Lambert, and R. J. Nichols, Precision control of single-molecule electrical junctions, Nat. Mater. **5**, 995 (2006).

[19] A. F. Takács, F. Witt, S. Schmaus, T. Balashov, M. Bowen, E. Beaurepaire, and W. Wulfhekel, Electron transport through single phthalocyanine molecules studied using scanning tunneling microscopy, Phys. Rev. B **78**, 233404 (2008).

[20] S. Schmaus, A. Bagrets, Y. Nahas, T. K. Yamada, A. Bork, M. Bowen, E. Beaurepaire, F. Evers, and W. Wulfhekel, Giant magnetoresistance through a single molecule, Nat. Nanotechnol. **6**, 185 (2011).

[21] A. Bagrets, S. Schmaus, A. Jaafar, D. Kramczynski, T. K. Yamada, M. Alouani, W. Wulfhekel, and F. Evers, Single molecule magnetoresistance with combined antiferromagnetic and ferromagnetic electrodes, Nano Lett. **12**, 5131 (2012).

[22] Y. Isshiki, S. Fujii, T. Nishino, and M. Kiguchi, Impact of junction formation processes on single molecular conductance, Phys. Chem. Chem. Phys. **20**, 7947 (2018).

[23] A. Vladyka, M. L. Perrin, J. Overbeck, R. R. Ferradás, V. García-Suárez, M. Gantenbein, J. Brunner, M. Mayor, J. Ferrer, and M. Calame, In-situ formation of one-dimensional coordination polymers in molecular junctions, Nat. Commun. **10**, 262 (2019).

[24] S. Hou, J. Zhang, R. Li, J. Ning, R. Han, Z. Shen, X. Zhao, Z. Xue, and Q. Wu, First-principles calculation of the conductance of a single 4,4 bipyridine molecule, Nanotechnology **16**, 239 (2005).

[25] C. J. Muller, J. M. van Ruitenbeek, and L. J. de Jongh, Conductance and Supercurrent Discontinuities in Atomic-Scale Metallic Constrictions of Variable Width, Phys. Rev. Lett. **69**, 140 (1992).

[26] S. A. G. Vrouwe, E. van der Giessen, S. J. van der Molen, D. Dulic, M. L. Trouwborst, and B. J. van Wees, Mechanics of lithographically defined break junctions, Phys. Rev. B **71**, 035313 (2005).

[27] J. P. Perdew, K. Burke, and M. Ernzerhof, Generalized Gradient Approximation Made Simple, Phys. Rev. Lett. **77**, 3865 (1996).

[28] S. Grimme, Semiempirical GGA-type density functional constructed with a long-range dispersion correction, J. Comput. Chem. **27**, 1787 (2006).

[29] S. Grimme, Accurate description of van der Waals complexes by density functional theory including empirical corrections, J. Comput. Chem. **25**, 1463 (2004).

[30] G. Kresse and J. Furthmüller, Efficient iterative schemes for *ab initio* total-energy calculations using a plane-wave basis set, Phys. Rev. B **54**, 11169 (1996).

[31] G. Kresse and J. Furthmüller, Efficiency of ab-initio total energy calculations for metals and semiconductors using a plane-wave basis set, Comput. Mater. Sci. **6**, 15 (1996).

[32] G. Kresse and J. Hafner, *Ab initio* molecular-dynamics simulation of the liquid-metal–amorphous-semiconductor transition in germanium, Phys. Rev. B **49**, 14251 (1994).

[33] G. Kresse and J. Hafner, *Ab initio* molecular dynamics for liquid metals, Phys. Rev. B **47**, 558 (1993).

[34] H. J. Monkhorst and J. D. Pack, Special points for Brillouin-zone integrations, Phys. Rev. B **13**, 5188 (1976).

[35] D. Frenkel and B. Smit, *Understanding Molecular Simulation: From Algorithms to Applications* (Elsevier, New York, 2001), Vol. 1.

[36] M. P. Allen and D. J. Tildesley, *Computer Simulation of Liquids* (Oxford University Press, New York, 2017).

[37] S. Nosé, A unified formulation of the constant temperature molecular dynamics methods, J. Chem. Phys. **81**, 511 (1984).

[38] N. Shuichi, Constant temperature molecular dynamics methods, Prog. Theor. Phys. Suppl. **103**, 1 (1991).

[39] W. G. Hoover, Canonical dynamics: Equilibrium phase-space distributions, Phys. Rev. A **31**, 1695 (1985).

[40] See Supplemental Material at http://link.aps.org/supplemental/10.1103/PhysRevB.104.L121407 for additional details about conductance measurements and analysis, jump to contact detection, correlation analysis, and theoretical calculations.

[41] M. Kamenetska, *Single Molecule Junction Conductance and Binding Geometry* (Columbia University, New York, 2012).

[42] J. Liu, X. Zhao, J. Zheng, X. Huang, Y. Tang, F. Wang, R. Li, J. Pi, C. Huang, L. Wang *et al.*, Transition from tunneling leakage current to molecular tunneling in single-molecule junctions, Chem **5**, 390 (2019).

[43] S. Y. Quek, M. Kamenetska, M. L. Steigerwald, H. J. Choi, S. G. Louie, M. S. Hybertsen, J. Neaton, and L. Venkataraman, Mechanically controlled binary conductance switching of a single-molecule junction, Nat. Nanotechnol. **4**, 230 (2009).

[44] T. Konishi, M. Kiguchi, M. Takase, F. Nagasawa, H. Nabika, K. Ikeda, K. Uosaki, K. Ueno, H. Misawa, and K. Murakoshi, Single molecule dynamics at a mechanically controllable break junction in solution at room temperature, J. Am. Chem. Soc. **135**, 1009 (2013).

[45] P. Makk, D. Tomaszewski, J. Martinek, Z. Balogh, S. Csonka, M. Wawrzyniak, M. Frei, L. Venkataraman, and A. Halbritter, Correlation analysis of atomic and single-molecule junction conductance, ACS Nano **6**, 3411 (2012).

[46] Z. Balogh, D. Visontai, P. Makk, K. Gillemot, L. Oroszlány, L. Pósa, C. Lambert, and A. Halbritter, Precursor configurations and post-rupture evolution of Ag-Co–Ag single-molecule junctions, Nanoscale **6**, 14784 (2014).

[47] C. Untiedt, A. I. Yanson, R. Grande, G. Rubio-Bollinger, N. Agraït, S. Vieira, and J. M. van Ruitenbeek, Calibration of the length of a chain of single gold atoms, Phys. Rev. B **66**, 085418 (2002).

[48] A. I. Yanson, G. Rubio Bollinger, H. E. Van Den Brom, N. Agraït, and J. M. Van Ruitenbeek, Formation and manipulation of a metallic wire of single gold atoms, Nature (London) **395**, 783 (1998).

[49] A. Magyarkuti, K. P. Lauritzen, Z. Balogh, A. Nyáry, G. Mészáros, P. Makk, G. C. Solomon, and A. Halbritter, Temporal correlations and structural memory effects in break junction measurements, J. Chem. Phys. **146**, 092319 (2017).

[50] Z. Balogh, P. Makk, and A. Halbritter, Alternative types of molecule-decorated atomic chains in Au–Co–Au single-molecule junctions, Beilst. J. Nanotechnol. **6**, 1369 (2015).

[51] M. R. Calvo, C. Sabater, W. Dednam, E. B. Lombardi, M. J. Caturla, and C. Untiedt, Influence of Relativistic Effects on the Contact Formation of Transition Metals, Phys. Rev. Lett. **120**, 076802 (2018).

[52] M. A. Fernández, C. Sabater, W. Dednam, J. J. Palacios, M. R. Calvo, C. Untiedt, and M. J. Caturla, Dynamic bonding of metallic nanocontacts: Insights from experiments and atomistic simulations, Phys. Rev. B **93**, 085437 (2016).